Enzymatic Tailor-Made Proteolysis of Whey in a Vortex Flow Reactor

Miriam M. Resende, Ruy Sousa Jr., Paulo W. Tardioli, Raquel L. C. Giordano, and Roberto C. Giordano
Departamento de Engenharia Química, Universidade Federal de São Carlos, São Carlos, SP, Brazil

DOI 10.1002/aic.10241
Published online in Wiley InterScience (www.interscience.wiley.com).

Enzymatic hydrolysis of cheese whey proteins with immobilized enzymes, providing a tailor-made pool of peptides, within narrow ranges of molecular weight, might be an advantageous alternative for this by-product of the dairy industry. In this work, Alcalase® was immobilized in agarose–glyoxyl gel beads and the proteolysis reaction was run in a continuous Taylor–Couette–Poiseuille reactor [or vortex flow reactor (VFR)], which presented efficient stirring without damaging the fragile beads. VFR mass transfer parameters were estimated after residence time distribution assays. Artificial neural networks were used to predict reaction rates of five ranges of peptide molecular weights. Using this hybrid model, a detailed description of the system was achieved. A bench-scale VFR (radius ratio $\eta = 0.48$ and aspect ratio $\Gamma = 11.9$) was used to validate the model.
 AIChE J, 21: 314–322, 2005
Keywords: Taylor–Couette–Poiseuille flow, immobilized enzyme, reactor modeling, cheese whey hydrolysis, artificial neural network

Introduction

Cheese whey is a byproduct of the dairy industry with high contents of lactose (~60 kg/m^3) and proteins (~6 kg/m^3, typically 56–60% w/w β-lactoglobulin, 18–24% α-lactoalbumin, 6–12% bovine serum albumin, and 6–12% immunoglobulins[1]). If discharged *in natura*, cheese whey is a deleterious effluent (30,000 BOD). Thus, recovering lactose and processing whey proteins may be an attractive alternative for the industry, increasing profits while reducing environmental costs.

The partial hydrolysis of cheese whey proteins with different proteases can either change or evidence functional properties of the resulting peptides. Hydrolyzed whey, containing mostly di- and tripeptides, is suitable for parental feeding. Whey protein hydrolysates can also be used as a protein source for individuals with reduced capacity of digestion and in bioactive peptides free from bitterness.[2] A controlled hydrolysis of whey can provide a mixture of peptides and amino acids with small contents of phenylalanine, fitted for the diet of phenylketonuria (PKU) patients (market prices approximately US$300.00/kg in powder form). Thus, the controlled whey proteolysis, besides being an environment-friendly approach, also aggregates considerable value to an otherwise problematic reject of the dairy industry.

Enzymatic proteolysis of whey, to be competitive, relies on the use of immobilized enzymes, which are generally supported on shear-sensitive matrices. Therefore, an industrial enzymatic reactor for this process should combine efficient mixing with low shear stresses.

Many authors have studied the use of Taylor–Couette flow[3] in chemical and biochemical reactors, the so-called vortex flow reactors (VFRs).[4-10] Taylor vortices are periodic flow patterns that appear in the gap between two concentric cylinders, the inner one rotating and the outer one usually stationary. When an axial (Poiseuille) flow is superimposed to the Taylor vortices, the system may be used as a continuous reactor. A particularly significant feature of VFRs is the low shear stress that Taylor flow provides.[9] The vortices ensure a gentle yet efficient agitation, particularly interesting for applications in bioprocesses.

The fluid dynamics of Taylor–Couette–Poiseuille (TCP)

Correspondence concerning this article should be addressed to R. C. Giordano at roberto@deq.ufscar.br.

flow, in the absence of end effects (that is, for an infinite-length apparatus) is characterized by three dimensionless parameters: the rotational (Re_θ) and the axial (Re_{ax}) Reynolds numbers, and the radius ratio ($\eta = R_{internal}/R_{external}$) of the apparatus (for an in-depth discussion of linear models of TCP flow, see Chandrasekhar[11]). The role of end effects is linked to a fourth parameter, the device aspect ratio ($\Gamma = L/d$). Anomalous patterns may occur for short devices (that is, for $\Gamma < 10$[12]), but VFRs usually have $\Gamma > 10$. Thus, theory indicates that the characteristic numbers Re_θ, Re_{ax}, and η could be the basis for the reactor scale-up. Certainly, scaling-up always poses specific problems, but a lab-scale VFR provides useful insights for building a sound mathematical model, a valuable tool supporting the design of the industrial reactor.

When fragile particles are present in the medium, Taylor flow shows certain advantages with respect to stirred-tank reactors. VFRs avoid the aggressive agitation of conventional impellers, and their power consumption is consequently lower than that of stirred tanks. The mixing provided by low-shear agitators (such as those used in animal cells cultivation) may not ensure proper fluidization of higher-density biocatalysts in agitated tanks. On the other hand, the rotation rate of the inner cylinder gives an additional degree of freedom for VFRs. When working with low-density biocatalysts, or even with soluble enzymes (homogeneous VFR), lower rotations will still sustain intravortex mixing, whereas intervortex mass transfer is reduced, and the reactor will approach a plug-flow behavior.

Mass transfer resistances through the external film, when processing large molecules such as proteins, may be overcome in VFRs when a convenient rotation of the internal cylinder is sustained. Even at these higher rotations, no damage is observed on the catalyst particles inside vortex reactors.

Packed-bed reactors typically present low interstitial velocities when hydrolyzing concentrated whey, and film resistances may become a problem. Finally, differently from fluidized-bed reactors, VFRs sustain suspended particles independent of the axial flow rates, thus avoiding recycling of the product stream.

Of course, VFRs have a drawback: they demand higher volumes (because of the internal cylinder dead volume). Nevertheless, when dealing with expensive, fragile particles (such as a biocatalyst), VFRs are a competitive alternative.

This paper presents a methodology that was able to deal with the complex problem of predicting the distribution of molecular weights of peptides at the outlet of a continuous flow enzymatic reactor. A mathematical model of a continuous VFR for the tailor-made proteolysis of cheese whey, which can be useful for process scale-up and optimization, was presented. In this work, the classical chemical reaction engineering approach is used: adoption of a simplified flow model; estimation of the model mass transfer coefficients using residence-time distribution experiments with an inert tracer; and definition of an apparent kinetic model (for the biocatalyst particles) from experiments in a batch reactor, in the absence of external mass transfer delays. Finally, the model is validated in independent experiments, with the VFR under actual operation.

The present system, however, poses some specific difficulties. The kinetic model is the most striking one. If one intends to fine-tune the size of the peptides that leave the reactor (the "tailor-made proteolysis"), an accurate prediction of the distribution of molecular weights is demanded. This task cannot be accomplished with the kinetic models available in the literature, which quantify the advance of proteolytic reactions in terms of the "degree of hydrolysis."[13]

Following the "degree of hydrolysis" approach, reaction rates are expressed as the number of hydrolyzed peptides bonds/time. These rates are then fitted either to a Michaelis–Menten equation (usually with a product inhibition term), or to a first-order kinetics. In the last case, the assumed rate-controlling step is the initial attack on the protein, which would open its structure for the subsequent reactions, the so-called zipper mechanism.[14]

Thus, in conventional proteolysis models, the concentrations of a complex mixture of substrates and products are lumped as a "concentration of peptide bonds that are available for hydrolysis," or as a "number of hydrolyzed bonds." This is indeed a very simplified picture of the system, if one recalls the huge number of reactions that occur when the enzyme is acting on a protein: depending on the specific link that is broken, different molecules are generated. When the hydrolysis of the resulting oligopeptides proceeds, a tree of possible reaction paths is revealed. A mechanistic model of this dimension would not be tractable.

"Degree of hydrolysis" models thus give no information regarding the molecular weight distribution (MWD) of the product, which is the most important variable in tailor-made proteolysis. To overcome this difficulty, a different approach was applied here. Five artificial neural networks (NNs) were trained to predict the rates of consumption/formation for each band of MW, as a function of the MWD of the peptides, at pH 7.0, 8.0, 9.0, and 10.0. These NNs were trained from independent batch assays in a pHstat.[15] At intermediate pH values, a linear interpolation with respect to 10^{pH} was used to calculate the reaction rates.

Therefore, in this work a classical mechanistic model for the continuous VFR[10] was coupled to NNs that predicted reaction rates of the peptides produced by the protease, lumped into five ranges of molecular weights. The mass transfer parameters for the continuous VFR were estimated after fitting residence time distributions (RTDs) of tracers, using conditions that emulate the reaction medium.

A bench-scale heterogeneous VFR, containing suspended particles in the gap between the cylinders, was used to validate the overall model. The biocatalyst was a proteolytic enzyme (Alcalase®), immobilized on agarose–glyoxyl gel beads through a multipoint covalent attachment.[16] Thus, simulated results provided by the hybrid model could be compared against data obtained from independent experiments in the VFR.

Experimental

Residence time distribution assays

The VFR was a jacketed glass vessel, with the inner cylinder made of polypropylene. Its radius ratio was $\eta = 0.48$ and the aspect ratio, $\Gamma = 11.9$. The VFR volume was 2.46×10^{-4} m^3 and the inner cylinder diameter was 2.6×10^{-2} m (gap width, 1.4×10^{-2} m). Rotation rates and reaction temperatures were controlled with aid of a microcomputer, and an interface unit from T&S (São Carlos, Brazil), with an accuracy of 0.1 s^{-1} and 1°C, respectively.

A Pharmacia P1 peristaltic pump circulated the medium. Particles [agarose gel, 6% w.b., $\phi_{av} = 55.0 \pm 9.0 \times 10^{-6}$ m,

apparent density in water 1080 ± 2 kg/m^3 (both values are means ± SD); Hispanagar, Spain] were continuously recycled to the VFR during the experiments. Working fluids were water at 38°C ($\mu = 7.60 \times 10^{-4}$ kg m^{-1} s^{-1} and $\rho = 993$ kg/m^3), replacing the hydrolyzed whey at 50°C, and a 14% w/w glycerol–water solution at 27°C ($\mu = 1.05 \times 10^{-3}$ kg m^{-1} s^{-1} and $\rho = 1030$ kg/m^3), emulating the concentrated raw cheese whey, also at 50°C. All viscosities were measured with a Brookfield viscometer (model DV-III). The tracers were blue dextran (Sigma), average MW 2×10^6 Da (molecular diffusivity 1.06×10^{-11} m^2/s, infinite dilution in water at 25°C; Moore and Cooney[25]) and methylene blue, Vetec, 373.9 Da (molecular diffusivity 1.66×10^{-10} m^2/s, infinite dilution in water at 25°C, estimated using the Wilke–Chang equation[17]). The first tracer cannot diffuse into the pores of the gel nor be adsorbed into the gel matrix, and was used to check how the particles might alter the mixing patterns of the liquid phase. A solution of blue dextran (2.0×10^{-7} m^3, 10 kg/m^3) was injected in the VFR; for methylene blue, the pulse volume was 5.0×10^{-8} m^3 (of a 5 kg/m^3 tracer solution). Each injection lasted for about 20 s, minimizing the dispersion of tracer to neighboring vortices during the pulse.

The VFR bed porosity was 98% (4.92×10^{-6} m^3 of particles/2.46×10^{-4} m^3 reactor). During experiments in the presence of particles, samples were collected at the VFR exit and analyzed using a Pharmacia UltraSpec 2000 spectrophotometer (280 nm for blue dextran and 665 nm for methylene blue), after separating the gel beads by gravity. The detector provided a linear response in this region. Collection times were always 50 s. In blank experiments (without particles), the outlet stream passed through a continuous-flow cell; samples were also collected, to cross-check the results. The hold-up volume of the tubing in the reactor outlet was less than 0.1% of the VFR volume. The minimum rotation of the inner cylinder that sustained homogeneous suspended particles in the medium at the reaction conditions was $\omega = 20.0$ s^{-1} ($\mathrm{Re}_\theta = 4759$, visual observation).

Enzyme immobilization

The biocatalyst was agarose gel, loaded with 7.8×10^3 U_{BAEE}/kg$_{\mathrm{gel}}$. Enzyme activity was expressed in benzoil arginine ethyl ester (BAEE) units: 1 U_{BAEE} was the amount of Alcalase® that hydrolyzed 1.0 μmol of BAEE per minute (at pH 8 and 25°C). The biocatalyst load in the VFR was 3.5×10^{-3} kg of beads.

The enzyme Alcalase® from Novo Nordisk (Bagsvaerd, Denmark) was covalently bonded to porous particles of agarose–glyoxyl gel 6% (weight basis; Hispanagar, Burgos, Spain), through multipoint links.[16,18,19] Glyceryl gels (agarose–O–CH_2–CHOH–CH_2OH) were produced after etherification of the agarose with glycidol (2,3-epoxypropanol). Further oxidization with sodium periodate provided glyoxyl-gels (agarose–O–CH_2–CHO). In a typical procedure, 1.50×10^{-4} m^3 of gel was suspended in 3.0×10^{-5} m^3 of distilled water. After that, 5.0×10^{-6} m^3 of a solution of NaOH 1.7 N with 28.5×10^3 kg/m^3 of sodium borohydride were added to the suspension. Glycidol was then slowly added, up to a final concentration of 2 M. The suspension was gently agitated for 18 h at 25°C. For oxidation, the glyceryl-gel was suspended in distilled water (1:10) and sodium periodate was added, up to 75.0 mol/(m^3 of gel), under mild stirring for 2 h. Further alcalase (amine)–agarose (aldehyde) multiple-point attachment was obtained by suspending the activated agarose gel in sodium bicarbonate buffer 50 mM, pH 10, in the proportion 1/10 ($V_{\mathrm{gel}}/V_{\mathrm{total}}$). Then, 1.0×10^{-1} m^3 of alcalase/m^3 of gel was added to the solution, which was maintained under gentle stirring for 24 h at 20°C. Sodium borohydrate (1.0×10^3 kg)/m^3 of solution was then added, over a period of 1800 s. Finally, the derivative was thoroughly washed with distilled water. The enzymatic activity difference of the supernatant, before and after immobilization, gave the gel load.

External mass transport resistance

To verify whether extraparticle mass transfer resistance was significant, a set of batch assays was carried out, in an 1.34×10^{-4} m^3 VFR. Five different rotations of the inner cylinder were studied (1.4, 5.2, 10.5, 20.9, and 52.3 s^{-1}), at 50°C. The catalyst load was 3.5×10^{-3} kg. The substrate was sweet cheese whey, donated by Cooperativa de Laticínios (São Carlos, Brazil). The whey was microfiltrated (membrane cutoff 0.45 μm; A/G Technology) and concentrated to 58.0 kg/m^3 in an ultrafiltration unit (membrane nominal cutoff 10,000 Da; Amicon).

Kinetic assays (batch assays in a pHstat)

Kinetic assays were accomplished in a 3.0×10^{-5} m^3 glass-jacketed vessel coupled to a pHstat (Titrino Metrohm). Concentrated cheese whey (58.0 kg/m^3: weight fractions of proteins: β-lactoglobulin, 56%; α-lactoalbumin, 20%; BSA, 11%; immunoglobulins and other fractions, 13%) was hydrolyzed at 50°C (Neslab thermostatic bath). The immobilized enzyme was added to the reactor at zero time, and the automatic control of pH (at 7.0, 8.0, 9.0, and 10.0) started at this time. Samples were periodically collected and analyzed using a size-exclusion column [Pharmacia Biotech Superdex™ Peptide HR 10/30 in a Shimadzu high-performance liquid chromatograph (HPLC)], with 0.25 M NaCl in 0.02 M phosphate buffer, pH 7.2, flow rate of 4.17×10^{-9} m^3/s, and detection at 214 nm.

Hydrolysis assays in the VFR with immobilized enzyme

All assays had $\mathrm{Re}_\theta = 3500$ and $\mathrm{Re}_{ax} = 1.10$. Concentrated cheese whey (58.0 kg/m^3) with sodium tetraborate (0.25 M) and NaOH (1.0 M) was fed to the reactor from a thermostatic bath (Neslab) at 50°C. The pH was adjusted to 9.5 and 2.20×10^{-4} m^3 of this solution was used in the jacketed reactor. The inner cylinder rotation was set to 20.9 s^{-1}.

The biocatalyst beads were kept in a 0.25 M sodium tetraborate/1.0 M NaOH buffer solution at pH 9.5, with 17% volume particles/volume buffer, under stirring. At the beginning of the assay, the gel was added to the reactor (up to 2% v/v). The feeding of gel (17% v/v) started immediately, to replace the loss at the VFR outlet, which was recycled to the reactor. The mass of gel in the VFR was measured at the end of the assay, and the steady-state regime was confirmed.

Proteolytic activities of the biocatalyst were always checked before and after each reaction assay in the VFR: 10 kg/m^3 solution of casein (Mallinckrodt Baker, Phillipsburg, NJ), was hydrolyzed in the pHstat (50°C at pH 9.5), 2.5 kg of casein/kg of gel. A typical result was an activity of (4.738×10^{-4} meq

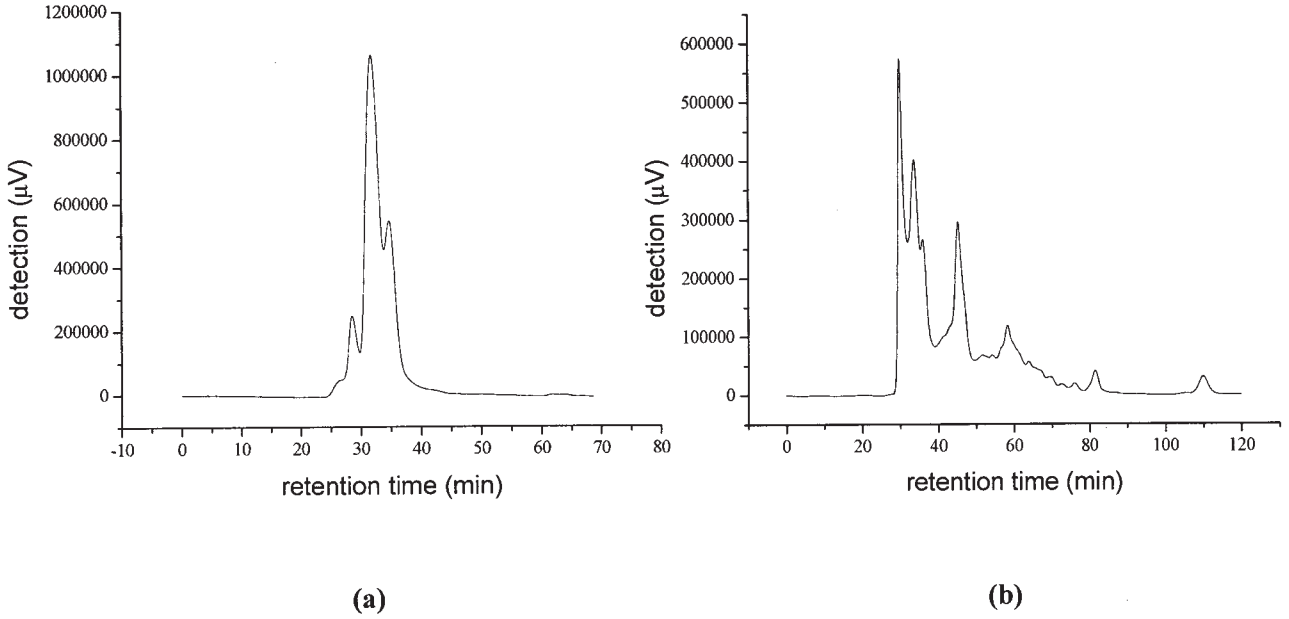

Figure 1. Illustrative chromatograms: column Superdex™ Peptide HR 10/30.

(a) Cheese whey, 50 g/m^3. (b) Products after 1120 s of proteolysis at pH 8, $T = 50$°C.

of base)/(g of casein × mL of gel). Enzyme deactivation after 24 h of operation of the VFR at 50°C was less than 1%. Enzyme losses from the biocatalyst were negligible in all assays, proving the stability of the multipoint attachments.

Analysis of the hydrolyzed whey

Samples were analyzed through HPLC, according to the procedure previously described. Five markers were used to define the MWD intervals of the products: BSA (67,000 Da, Sigma); β-lactoglobulin (18,000 Da, Sigma); insulin (5000 Da, Biobras); angiotensin II (Asp-Arg-Val-Tyr-Ile-His-Pro-Phe; MW 1046.7 Da, Sigma); and leucine enkephalin (Tyr-Gly-Gly-Phe-Leu; 555.6 Da, Sigma). The chromatographic analytic methodology is detailed elsewhere.[15] Typical chromatograms are shown in Figure 1.

Reactor model

A detailed description of the VFR mathematical model is reported in Giordano et al.,[10] which is a general model, holding either for moving or for stagnant vortices. All experiments reported in this work had the VFR operating at a high Re_θ/Re_{ax} ratio (≈3180 for the conditions at the reactor inlet). In this situation, the vortices do not move downstream (the so-called stagnant vortices), despite the axial flow. For the sake of brevity, the model equations presented here are already simplified, for stagnant vortices. This concept of vortex flow is pictured schematically in Figure 2.

Each control volume i includes a vortex core and the neighboring bypass region. Therefore, the (isothermal) model equations of Giordano et al.[10] reduce to:

Mass Balance for Component j in the ith Stage Bypass Region

$$V_i^e \frac{dC_{j,i}^e}{dt} = U_{ax}A(C_{j,1-1}^e - C_{j,i}^e) + 2\Delta_j A\left[\frac{(C_{j,i+1}^e - C_{j,i}^e)}{(z_{i+1} - z_{i-1})} - \frac{(C_{j,i}^e - C_{j,1-1}^e)}{(z_{i+1} - z_{i-2})}\right] - k_j S_i^v (C_{j,i}^e - C_{j,i}^v) + r_{j,i}^e V_i^e \quad (1)$$

Mass Balance for Component j in the ith Stage Vortex Core

$$V_i^v \frac{dC_{j,i}^v}{dt} = k_j S_i^v (C_{j,i}^e - C_{j,i}^v) + r_{j,i}^v V_i^v \quad (2)$$

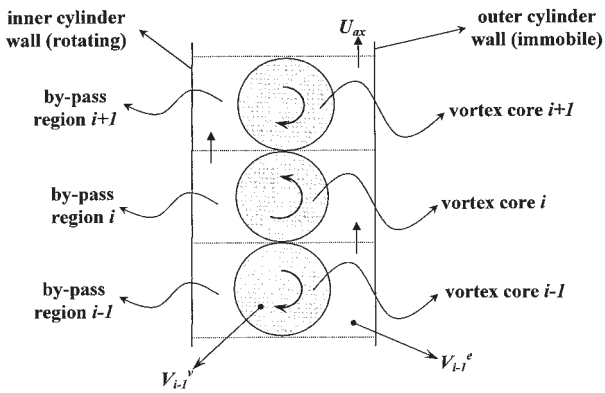

Figure 2. VFR model.

where V_i^v is the volume of a circular-section toroid, and V_i^e is the difference between the volume of the ith stage (a cylindrical annulus) and the volume of the toroidal vortex core.

According to this model:

- The net axial flow of fluid and particles would occur only along the bypass stream, and the vortices would be stagnant regions.
- The first term in the right-hand side (rhs) of Eq. 1 stands for the convective net flow (all through the bypass region).
- Axial dispersion effects and a possible countercurrent convective flow along the bypass stream are lumped in parameter Δ_j. A finite-differences approach is used to approximate these two phenomena and each stage is considered as an elemental volume, which results in the second term in the rhs of Eq. 1.
- Mass transport of component j between the vortex core and bypass flow is governed by the mass transfer coefficient k_j (third term in rhs of Eq. 1 and first term in rhs of Eq. 2).
- The rate term rV closes the balances.
- Boundary conditions for Eq. 1 emulated the classical equations for one-dimensional, axial dispersion models (entrance, at $z = 0$, referred to a concentration infinitely distant from the inlet, and exit with null concentration gradient, in backwards finite difference).

This is a transient-state model, used to predict the start-up of the VFR in continuous operation, up to its steady state. The five pseudocomponents j of the system, whose mass balances were solved, corresponded to five groups of peptides MW: >14.000, 14,000–4150, 4150–1050, 1050–650, <650 Da.

Parameters k and Δ were estimated from RTD data, and assumed equal for all components. The software of Giudici,[20] which uses the algorithm of Marquardt,[21] was used for that purpose, providing estimates of the covariance matrix of the parameters. The model equations were solved numerically, with a Runge–Kutta algorithm.[22]

Kinetic model

The multilayer perceptron (MLP) is one specific class of artificial neural networks (NNs), consisting of interconnected layers of processing units (neurons). Information goes forward, from one layer to the next. A MLP has an input and an output layer, and n hidden layers. Neurons in adjacent layers are linked by weighted connections. Each neuron is a processing element that initially sums the weighted signal coming from the previous layer plus an offset term (bias). Then a (generally) nonlinear transfer function evaluates the neuron output. In this work, the sigmoid function was used.

The process of finding an optimum set of weights for the connections is called learning. The back-propagation algorithm,[23] combined with a random-search procedure, was used in this work, using in-house software in FORTRAN. Nevertheless, several commercial softwares are available for this purpose (such as NN toolbox from MATLAB; The MathWorks, Natick, MA). Standard procedures[24] were used to define the network topology (number of hidden layers and number of neurons in it), and the number of training steps, from a set of validation data.

The root mean square (RMS) of the errors was the objective function to be minimized. The training data had 42 sets, and 18 sets were put away for validation. The NN topology was chosen to avoid overfitting: the RMS of the validation data should be minimal. The experimental data used for training the NN were obtained from batch hydrolysis assays in a well-mixed reactor, connected to a pHstat. Samples were periodically withdrawn and analyzed by size-exclusion chromatography. The resulting NN had five input neurons (the concentrations of each pseudocomponent, corresponding to the MW intervals) and five output neurons (the reaction rates of each pseudocomponent). The number of neurons in the hidden layer, taken from Sousa et al.,[15] was 40 (pH 7), 45 (pH 8), 48 (pH 9), and 48 (pH 10). For intermediate pH values, the reactions rates were linearly interpolated with respect to 10^{pH}. Figure 3 illustrates the quality of the NN fitting.

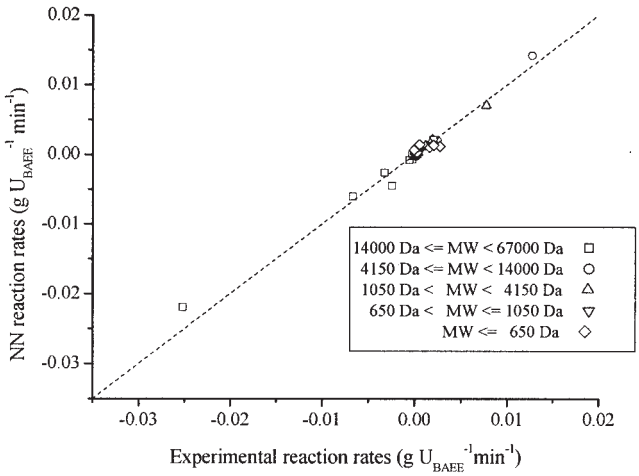

Figure 3. Validation test of the four neural networks used to model the kinetics of the proteolysis.

Temperature 50°C; pH 7, 8, 9, and 10.

The NNs thus calculate the reaction rate of each species (r_j in Eqs. 1 and 2), if the local concentrations of all components are known. In other words, the NNs work exactly as any classical rate equation (such as first-order or Michaelis–Menten). They were included as functions in the computer code, coupled to the mass balance equations.

It should be stressed here that a NN is a strictly empirical model. When dealing with a complex substrate such as cheese whey, extrapolation of the NN predictions is not advisable. Nevertheless, the methodology put forth here can be quickly implemented as a routine lab procedure, and the NNs can be retrained for the substrate that is processed in each individual industry.

Results and Discussion

VFR mass transfer parameters

Figure 4 is a typical response to a tracer pulse, demonstrating that there was no noticeable difference between the RTD for different tracers. This behavior is in agreement with the literature. Moore and Cooney[25] observed that VFR axial dispersion parameters were not sensitive to the coefficient of molecular diffusion of the tracer.

Figure 4 also shows that there was no significant change in the RTD when the reactor had 2% v/v of gel beads, indicating that the presence of suspended biocatalyst particles did not

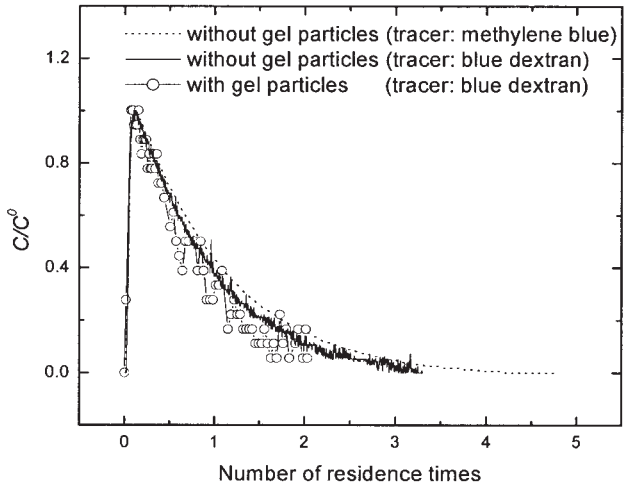

Figure 4. Experimental residence time distributions.

Pulses of blue dextran and methylene blue. VFR without particles and with 2% v/v of agarose gel. Water 38°C, Re_{ax} = 1.5, Re_θ= 11,782, Re_θ/Re_{ax} = 7855, τ = 1800 s.

change the VFR mass transfer characteristics, at least for the high bed porosity used here (98%).

Figure 5 illustrates the fitting of the model (Eqs. 1 and 2, without the reaction term) to experimental RTDs. A simulated pulse of tracer (10 s) disturbed the system, and concentrations were calculated using the model for all the stages (vortex cores and bypass regions). Model responses shown in Figure 5 were exit concentrations, coming from the bypass region of the top stage. In Figure 5a, the rotation rate of the inner cylinder was low, and Re_θ/Re_{ax} = 696. This value is not high enough to stop the downstream displacement of the vortices, and the discontinuities that can be noticed in the model response (see Figure 5a) correspond to the collapse of the upper vortices (for more details, refer to Giordano et al.[10]). Figure 5b exemplifies a typical RTD for immobile vortices. In this case, Re_θ/Re_{ax} = 3113 and all the net axial flow occurs circumventing the vortices. The model response is smooth because there are no collapses at the top of the apparatus.

Figures 5a and b also display the standard deviation of the parameters and their correlation coefficient. As expected, for the higher rotation rate (Figure 5b), the confidence intervals were broader. This is an indication that the VFR is gradually approaching the behavior of a perfectly mixed continuously stirred tank reactor (CSTR) and, consequently, a model with two parameters gradually becomes overparameterized. Nevertheless, the fitting is quite accurate. By using two parameters a general model is obtained that would span all the reactor operational conditions (including low Re_θ). Therefore, the two-parameter model was adopted hereon, even for high rotation rates of the inner cylinder.

Another aspect that deserves mention is the negative correlation between k and Δ. This is a typical behavior (an overestimation of k would imply a compensatory underestimation of Δ, and vice versa). The correlation between the parameters increases with Re_θ, which is in accordance with the discussion in the previous paragraph.

As previously reported, two solutions were used to bracket the operational conditions of the actual reactor (at 50°C). The first one emulates the properties of concentrated raw cheese whey, at the reactor inlet (using glycerol/water 14% w/w at 27°C, with $\mu = 1.02 \times 10^{-3}$ kg/ms). The second one (using pure water at 38°C, $\mu = 7.3 \times 10^{-4}$ kg/ms) corresponds to a mixture of peptides at the reactor outlet, also at 50°C. The Reynolds numbers were, respectively, Re_θ = 3334 and 4670; Re_{ax} = 1.1 and 1.5; and the ratio Re_θ/Re_{ax} was between 3031 and 3113, which is actually a small range. Careful simulations have shown that average values of the parameters (invariant throughout the VFR) could be used in this range of Reynolds numbers. Therefore, the simulations with the hybrid model were performed adopting $k = 1.7 \times 10^{-4}$ m/s and $\Delta = 4.4 \times 10^{-5}$ m^2/s.

External resistance to mass transfer

Figure 6 shows results of the experiments designed to check the importance of the resistance to mass transfer through the

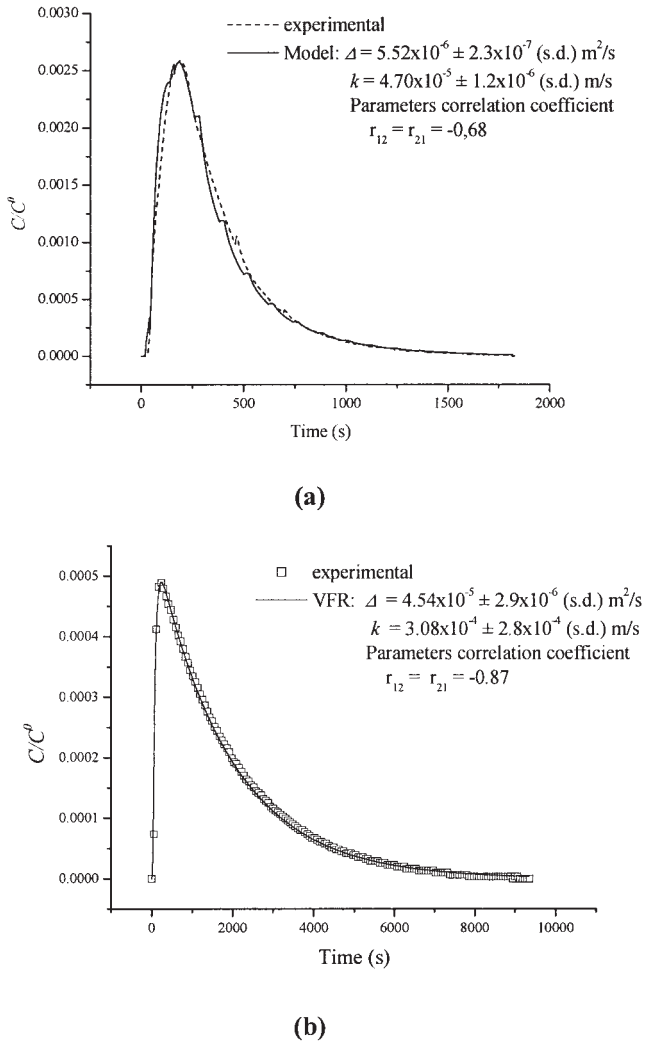

Figure 5. Pulse injections of methylene blue (VFR without particles): experimental and model results.

(a) Fluid: glycerol/water 4.2 M, 24°C. Re_{ax} = 0.47, Re_θ = 327.0; Re_θ/Re_{ax} = 696, τ = 200 s. Flow pattern for case (a): vortices move downstream and collapse at the VFR outlet and inlet. Details of the model for moving vortices are in Giordano et al.[10] (b) Fluid: water, 38°C. Re_{ax} = 1.50, Re_θ = 4670, Re_θ/Re_{ax} = 3113, τ = 1800 s. Flow pattern for case (b): stationary vortices, Eqs. 1 and 2.

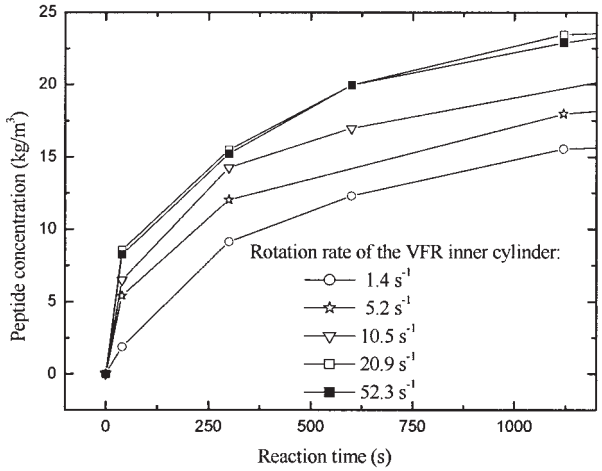

Figure 6. Testing the presence of external resistances to mass transfer. Batch assays in the VFR, for different rotation rates of the inner cylinder.

Bioparticle: agarose gel (55×10^{-6} m) with multipoint-attached alcalase. Substrate cheese: whey concentrate, 52 kg/m^3. Medium with sodium tetraborate buffer 0.25 M/NaOH 1.0 M at pH 9.5 and 50°C.

extraparticle film. It should be noted that particle fluidization was not uniform for the smaller rotation rates shown in this plot.

Samples were taken during batch runs in the VFR. The evolution of the total concentration of hydrolyzed peptides (measured by size-exclusion chromatography in a HPLC; see Experimental section) was assessed for different rotations rates of the internal cylinder. The results in Figure 6 show that above 20.9 s^{-1} (200 rpm) external film resistance became negligible. Thus, the rotation used thereon in the experiments with immobilized enzyme was 200 rpm.

Model validation

The hybrid model was used to simulate the VFR under continuous operation. The concentrations of five pseudocomponents were calculated, corresponding to MW ranges (in Da) of $\leq$650, 650–1050, 1050–4150, 4150–14,000, and $>$14,000. The NN provided the reaction rates r_j for each pseudocomponent. Results of typical validation runs are displayed in Figures 7 and 8. It should be noticed that these results correspond to pH 9.5; that is, the reaction rates were interpolated (using the pH 9 and 10 NNs). This is a strong validation test: if a neural network were trained specifically at pH 9.5, the fitting would certainly be improved.

It is evident that the model was able to capture the main features of this complex problem, predicting the concentrations of the substrate (cheese whey concentrate) and of the five ranges of peptides' MW. A qualitatively adequate representation of the VFR trajectory after the process start-up was obtained, and the steady states could also be predicted. The largest absolute offsets between experiment and model predictions at steady state were for 4150 $<$ MW $<$ 14,000 ($\sim +1.6$ kg/m^3), and for MW $>$ 14,000 (~ -1.6 kg/m^3) (see Figure 8). All other errors were much lower. This is quite an acceptable result, if one keeps in mind the drastic simplifications that were assumed, and the experimental uncertainties that are present

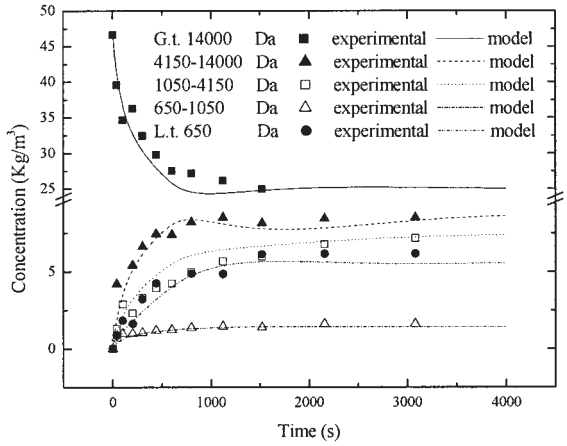

Figure 7. Model validation: concentrations of substrate and products after startup of the VFR.

Enzyme load: 3.5×10^{-3} kg of beads with 7.8×10^3 U_{BAEE}/kg_{gel}. Temperature 50°C, pH 9.5, τ = 1800 s.

when the complex mixture of peptides produced by the proteolysis is lumped into a few ranges of MW. It should be noted that the model satisfies the overall mass balance.

One important point in this discussion is whether a simpler flow model might describe this system. In fact, the complexity of the Taylor reactor model is directly linked to the rotation rate of the inner cylinder. At higher rotations, the VFR approaches a CSTR and, at lower rotations, a plug-flow reactor. Thus, a generic model of the VFR should span all intermediate operational conditions. For a specific application, the rotation must be defined by also taking into account the apparent densities of the particles (usually a gel matrix): lighter particles would demand lower rotation rates for minimum fluidization, and the VFR could operate closer to a plug flow; inversely, denser particles might conduct to an (almost) ideal CSTR behavior. In other words, the choice of the matrix used for enzyme immobilization may ultimately determine the fluid dynamics of the

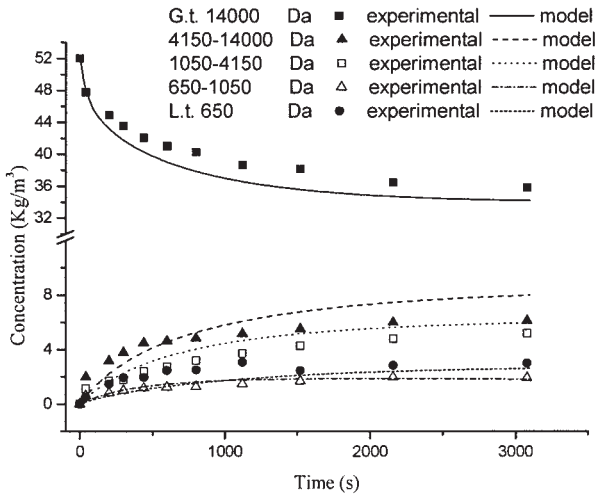

Figure 8. Model validation: concentrations of substrate and products after startup of the VFR.

Enzyme load: 1.0×10^{-3} kg of beads with 7.8×10^3 U_{BAEE}/kg_{gel}. Temperature 50°C, pH 9.5, τ = 1500 s.

reactor, and its model must account for these different possibilities.

Conclusions

The controlled proteolysis of cheese whey could be successfully accomplished on a continuous vortex flow reactor, using a glyoxil–agarose–alcalase biocatalyst. Conventional models of the hydrolysis of proteins cannot predict the distribution of molecular weight of the products. Nevertheless, this information is crucial for a successful tailor-made hydrolysis (that is, when one wishes to control the MWD of the product within narrow ranges). In this work, a hybrid model (phenomenological-neural network) was developed, which predicted the distribution of MW at the reactor outlet. The model was successfully validated against independent experiments, predicting start-up transients and steady-state operation as well. Thus, it may be used to design and optimize the proteolysis, changing reactor residence times and pH values. Fine-tuning of the peptides' MWD can be accomplished using different enzymes in series, such as trypsin (for an initial attack on the whey), chymotrypsin, and carboxypeptidase A (to reduce phenylalanine contents, when producing food for PKU patients). All these reactions can be simulated using the approach described here, provided sufficient experimental data are available to train the neural networks.

It was observed that the presence of suspended biocatalyst particles did not change the VFR mass transfer characteristics, at least for the high bed porosity used here (98%). At rotation rates above 200 rpm ($\mathrm{Re}_\theta > 3334$), the mass resistance through the external film of the biocatalyst beads became negligible. Despite the variation of the medium viscosity during the course of the proteolysis (from about 1.0×10^{-3} to about 7.3×10^{-4} kg m^{-1} s^{-1}), average values for the mass transfer parameters could be used to simulate the VFR. The reactor model was able to represent the RTD curves in all the situations of interest for the hydrolytic process.

A favorable agreement with the experimental concentrations of substrate (cheese whey concentrate) and of product (five ranges of peptides' MW) was achieved. Both the transient (after start-up) and the steady state of the VFR could be predicted. Running the reaction in the VFR provided an independent validation of the model, given that mass transfer parameters and the reaction kinetics were assessed through independent experiments, and the VFR conversions were not used to fit any parameter. The artificial neural network was able to map the reaction course, providing details concerning the distribution of molecular sizes of the peptides, which are of extreme utility to design the tailor-made hydrolyses of proteins.

Acknowledgments

The authors gratefully acknowledge the support of the Brazilian research funding agencies FAPESP and CNPq.

Notation

A = VFR annular cross section, m^2
C = VFR outlet concentration of tracer, kg/m^3
C^0 = tracer mass/VFR volume (pulse injection), kg/m^3
$C^e_{j,i}$ = concentration of component j in the bypass region of stage i, kg/m^3
$C^v_{j,i}$ = concentration of component j inside vortex i, kg/m^3
d = reactor gap ($R_{\mathrm{external}} - R_{\mathrm{internal}}$), m
k_j = vortex-bypass mass transfer coefficient of component j, m/s
L = axial length of the reactor, m
$r^e_{j,i}$ = rate of reaction of component j in the bypass region of vortex i, kg/m^3s
$r^v_{j,i}$ = rate of reaction of component j in vortex i, kg/m^3s
Re_θ = rotational Reynolds number ($=\omega R_i d/\nu$)
Re_{ax} = axial Reynolds number ($=U_{ax}d/\nu$)
S^v_i = external surface of the toroidal vortex i, m^2
t = time, s
U_{ax} = superficial velocity, m/s
V^e_i = volume of the bypass region of stage i, m^3
V^v_i = volume of vortex core i, m^3

Greek letters

Γ = aspect ratio ($=L/d$)
Δ_j = bypass axial dispersion coefficient of component j, m^2/s
η = radius ratio ($=R_{\mathrm{internal}}/R_{\mathrm{external}}$)
τ = mean residence time, s
ν = kinematic viscosity, m^2/s

Literature Cited

1. Morr CV, Ha EYW. Whey-protein concentrates and isolates—processing and functional-properties. *Critical Reviews in Food Science and Nutrition.* 1993;33:431-476.
2. Mann E. Whey products and their uses. *Dairy Industry International.* 2000;December:13-14.
3. Taylor GI. Stability of a viscous liquid contained between two rotating cylinders. *Philosophical Transactions of the Royal Society of London Series A: Physical Sciences* 1923;223:289-343.
4. Cohen S, Maron DM. Analysis of a rotating annular reactor in the vortex flow regime. *Chemical Engineering Science.* 1991;46:123-134.
5. Kataoka K, Ohmura N, Kouzu M, Simamura Y, Okubo M. Emulsion polymerization of styrene in a continuous Taylor vortex flow reactor. *Chemical Engineering Science.* 1995;50:1409-1416.
6. Sczechowski JG, Koval CA, Noble RDF. A Taylor vortex reactor for heterogeneous photocatalysis. *Chemical Engineering Science.* 1995; 50:3163-3173.
7. Leitner NKV, Le Bras E, Foulcault E, Bousgarbiès J-L. A new photochemical reactor design for the treatment of absorbing solutions. *Water Science Technology.* 1997;35:215-222.
8. Ameer GA, Harmon W, Sasisekharan R, Langer R. Investigation of a whole blood fluidized bed Taylor–Couette flow device for enzymatic heparin neutralization. *Biotechnology and Bioengineering.* 1999;62: 602-608.
9. Giordano RLC, Giordano RC, Cooney CL. Performance of a continuous Taylor–Couette–Poiseuille vortex flow enzymic reactor with suspended particles. *Process Biochemistry.* 2000;35:1093-1101.
10. Giordano RC, Giordano RLC, Prazeres DMF, Cooney CL. Analysis of a Taylor–Poiseuille vortex flow reactor—II: Reactor modeling and performance assessment using glucose–fructose isomerization as test reaction. *Chemical Engineering Science.* 2000;55:3611-3626.
11. Chandrasekhar S. *Hydrodynamic and Hydromagnetic Stability*. Oxford, UK: Clarendon Press; 1961.
12. Koschmieder EL. *Bénard Cells and Taylor Vortice*s. New York, NY: Cambridge Univ. Press; 1993.
13. Adler-Nissen J. Enzymic hydrolysis of food proteins. New York, NY: Elsevier Applied Science; 1986.
14. Vorob'ev MM, Levicheva IYU, Belikov VM. Kinetics of the initial stage of milk protein hydrolysis by chymotrypsin. *Applied Biochemistry and Microbiology.* 1996;32:219-222.
15. Sousa R Jr, Resende MM, Tardioli PW, Giordano RLC, Giordano RC. Hybrid model of an enzymatic reactor: hydrolysis of cheese whey proteins by alcalase immobilized in agarose gel particles. *Applied Biochemistry and Biotechnology.* 2003;105/108:413-422.
16. Tardioli PW, Pedroche J, Giordano RLC, Fernandez-Lafuente R, Guisan JM. Hydrolysis of proteins by immobilized-stabilized alcalase glyoxyl-agarose. *Biotechnology Progress*. 2003;19:352-360.
17. Reid RC, Prausnitz JM, Poling BE. *The Properties of Gases and Liquids* (4th ed.). New York, NY: McGraw-Hill International; 1988.

18. Guisan JM. Aldehyde-agarose gel as actived supports for immobilization-stabilization of enzymes. *Enzyme Microbiology Technology.* 1988;10:375-382.
19. Blanco RM, Guisan JM. Stabilization of enzymes by multipoint covalent attachment to agarose-aldehyde gels. Borohydride reduction of trypsin-agarose derivates. *Enzyme Microbiology Technology.* 1989;11: 360-366.
20. Guidici R. *DMARQ: Software for Estimation of Parameters in Differential Models*; internal report 1990.
21. Marquardt DW. An algorithm for least-squares estimation of nonlinear parameters. *Journal of the Society for Industrial and Applied Mathematics.* 1963;11:431-441.
22. Press WH, Teukolsky SA, Vetterling WT, Flannery BP. *Numerical Recipes in Fortran 90* (2nd ed.). New York, NY: Cambridge Univ. Press; 1996.
23. Rumelhart DE, Hinton GE, Williams RJ. Learning representations by back-propagating errors. *Nature*. 1986;323:533-536.
24. Baughman DR, Liu YA. *Neural Networks in Bioprocessing and Chemical Engineering*. New York, NY: Academic Press; 1995.
25. Moore CMV, Cooney CL. Axial dispersion in Taylor–Couette flow. *AIChE Journal.* 1995;41:723-727.

Manuscript received Nov. 6, 2002, and revision received Apr. 23, 2004.